Available online at www.sciencedirect.com
ScienceDirect

Fire Safety Journal 42 (2007) 1–10

FIRE SAFETY JOURNAL

www.elsevier.com/locate/firesaf

Nonlinear analysis of SRC columns subjected to fire

Jiang-Tao Yu*, Zhou-Dao Lu, Qun Xie

Research Institute for Structural Engineering and Disaster Reduction, Tongji University, Shanghai 200092, China

Received 14 June 2005; received in revised form 16 March 2006; accepted 20 June 2006
Available online 25 October 2006

Abstract

Both experimental and numerical methods were employed to investigate the behavior of steel reinforced concrete (SRC) columns subjected to fire. Twelve specimens were tested at ambient and elevated temperatures. A procedure was developed to predict the temperature distribution and ultimate strength of the SRC columns subjected to fire by following certain assumptions. In the procedure, a combined method of finite element and finite-difference was adopted to analyze the temperature distribution, and the responses of the SRC columns under loads were predicted by the procedure both at ambient temperature and elevated temperatures. To illustrate the problem and verify the accuracy of the predictions, we present a few comparisons between the test data and calculated results. At the end of the paper, equations for the ultimate strength of the SRC columns subjected to fire were obtained by a regression analysis.

Keywords: Steel reinforced concrete; Elevated temperatures; Temperature distribution; Finite element method; Ultimate strength

1. Introduction

A steel reinforced concrete (SRC) member is a structural combination of three kinds of materials: steel section, steel reinforcement and concrete. Due to their outstanding load bearing capacities, SRC members are widely used in high-rise buildings.

It is known that the failure of structural members in fire is mainly caused by the failure of their inner steel components. Compared with normal reinforced concrete (NRC), the SRC members have less fire resistance for their higher steel ratio. This paper is aimed at raising the nationwide awareness of the fire resistance of SRC columns:

1) to describe the experiments of the SRC columns in different conditions;
2) to predict the temperature distribution of a SRC column subjected to fire;
3) to find a numerical method to predict the responses of a SRC column subjected to fire;
4) to verify the accuracy of the calculation and derive equations to describe the ultimate strength of a SRC column subjected to fire.

2. Experimental programs

2.1. Specimen preparation

In this paper, the word "column" or "specimen" means SRC column.

Twelve columns were constructed for experiment, six of which were tested at ambient temperature and the rest were at elevated temperatures. Fig. 1 shows the dimensions of the cross-section and locations of thermocouples (to make the figure clearer, stirrups are not shown).

2.1.1. Material properties

Strips of the steel sections and steel reinforcement were tested in tension according to the Chinese standard GB2975 [1]. The average yield strength (f_{sy}) of the steel section was found to be 280.5 MPa and the modulus of elasticity (E_s) was about 206,000 MPa. The average yield stress of steel reinforcement (f_y) was 351.4 MPa and the modulus of elasticity (E_s) was about 210,000 MPa.

*Corresponding author.
E-mail address: maverickgrit@hotmail.com (J.-T. Yu).

0379-7112/$ - see front matter
doi:10.1016/j.firesaf.2006.06.006

Nomenclature

A_c	concrete cross-sectional area
A_s	steel cross-sectional area
B	cross-sectional width
C	specific heat
H	cross-section height
e_0	value of eccentricity
$[K]$	temperature stiffness matrix
L	length of the SRC column
M	moment
N	axial force
N_{ct}	ultimate strength at given time
N_{co}	ultimate strength at ambient temperature
N_{c7}	ultimate strength with $\lambda = 7$
N_{20}	ultimate strength with initial eccentricity
$[N]$	temperature-change matrix
$\{P\}$	column vector
q_c	heat flow density
q_r	radiation heat transfer
T	temperature
t	fire duration time
β	thermal conductivity
ε	stain
ε_r	surface emissivity
φ	curvature
η_e	eccentric ratio
λ	slenderness ratio
ρ	density of material
σ	Stefan-Boltzman constant

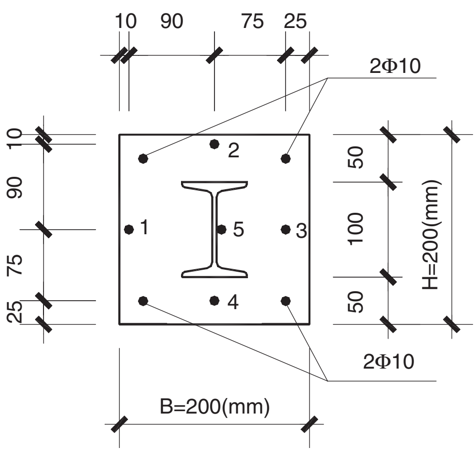

Fig. 1. Location of the thermocouples (numbered 1–5) in the cross-section.

The concrete mix was designed for a compressive cubic strength (f_{cu}) at 28 days of 39.9 MPa, and the average value of the elastic modulus (E_c), which was about 33,000 MPa, was measured in accordance with the Chinese standard GBJ81-85 [2]. The mix proportions of cement: fine aggregate: coarse aggregate is equal to 1:1.09:2.95, while the value of water: cement ratio is 0.43. In all the concrete mixes, the fine aggregate used was silica-based sand, and the coarse aggregate was calcareous stone (Table 1).

2.1.2. Specimens

More details of the specimens are shown in Figs. 1, 3 and 4. As to the columns tested at ambient temperature, the loads were applied in increments of 1.5 kN/s, until the columns failed. The load (300 kN) applied to the columns in fire was kept constant, while the temperature was increased according to Eq. (2) (see Fig. 2).

2.1.3. Fire exposure and test apparatus

Five displacement transducers were used to measure the transverse deformation in the test region (shown in Fig. 3). Stain gauges, which were installed at the surface of steel section and reinforcement, were applied to determine the longitudinal strain of specimens.

The temperatures were measured by five calibrated thermocouples fixed inside the cross-section of the specimens. The locations of the thermocouples are shown in Fig. 1.

The principle of the loading regime is to apply temperature increments under constant load. Two 300 kN hydraulic jacks controlled by a DCZ-1 electronic scale provided a constant load of 300 kN. In the process of experiment, a DH3815 static strain collection system recorded, every 5 min, the strain and transverse deformation of specimens, while a multi-point recorder was recording the changes of temperature automatically. Fig. 2 shows the increasing temperature of the furnace.

The specimens were tested in a furnace of the Fire-Resistance Laboratory, Tongji University, China. The ambient temperature at the beginning of the test was about 20 °C. Two sides (near No. 1 and No. 3 thermocouples) of the columns were exposed to the naked flame, and the other two were heated by hot gas.

The ISO-834 standard fire curve can be expressed as [3]:

$$T_g = 345 \log(8t + 1) + T_0, \tag{1}$$

in which t denotes the time (min); T_g is the furnace temperature (°C) at time t, and T_0 is the ambient temperature (°C).

Temperature curves of the furnace were recorded according to the Chinese standard GB9978-88 [4]. The heating curve was kept as close as possible to the ISO-834 standard fire curve. However, the ideal condition could not be reached due to certain limitations in the experimental setup. Fig. 2 presents both the standard curve and the actual one, which is the average of all six specimens. The actual curve can be expressed by a

Table 1
Summary of specimen information

Specimen number	Section size $B \times H \times L$ (mm)	Reinforcement (mm)	Stirrup (mm)	Steel section	Eccentricity of load (mm)
SRC1.4-0	$200 \times 200 \times 1400$	4Φ10	Φ6.5@100	I 10	0
SRC1.4-40		4Φ10	Φ6.5@100	I 10	40
SRC1.4-80		4Φ10	Φ6.5@100	I 10	80
SRC1.4-0	$200 \times 200 \times 1800$	4Φ10	Φ6.5@100	I 10	0
SRC1.4-40		4Φ10	Φ6.5@100	I 10	40
SRC1.4-80		4Φ10	Φ6.5@100	I 10	80

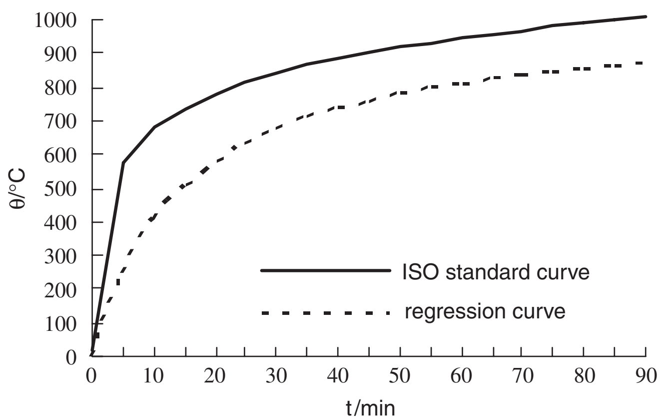

Fig. 2. Relation of temperature versus time.

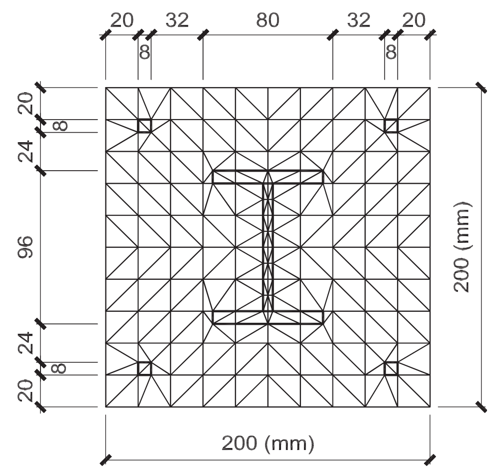

Fig. 4. Elements of the cross-section.

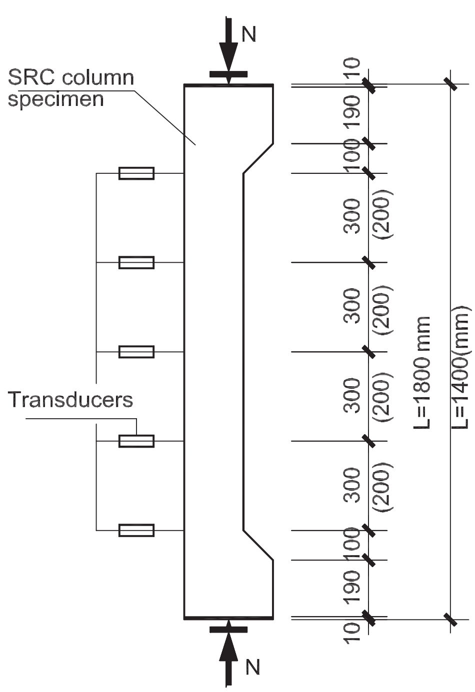

Fig. 3. Arrangement of tests.

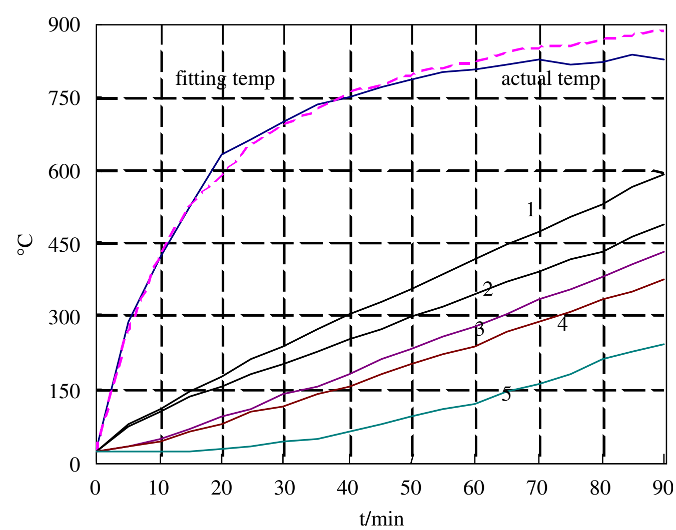

Fig. 5. Temperature versus time curve.

regression equation as

$$T_g = \frac{1008.5t}{15 + t} + T_0, \tag{2}$$

Parts of the test data are shown in Figs. 5–10 and Figs. 12–19 along with the calculated results.

3. Analysis of the temperature distribution

To predict the responses of a SRC column subjected to fire, a procedure called prediction of temperature distribution and damage (PTDD) of SRC columns was developed. The coefficients concerned with the calculation of temperature distribution are as follows:

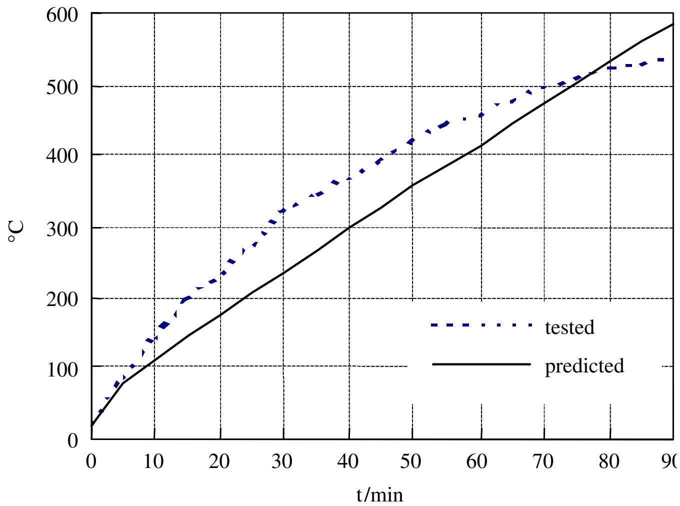

Fig. 6. Comparison of temp–curve (point 1).

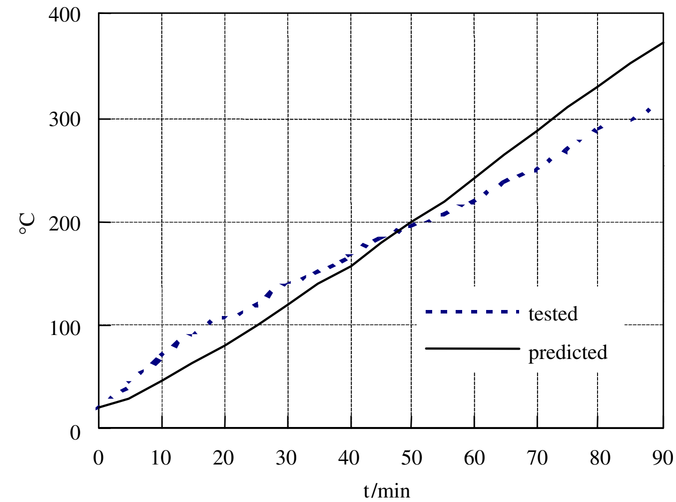

Fig. 9. Comparison of temp–curve (point 4).

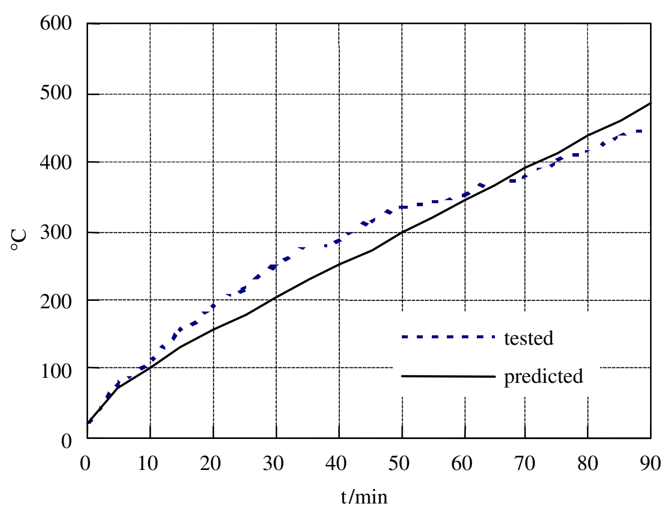

Fig. 7. Comparison of temp-curve (point 2).

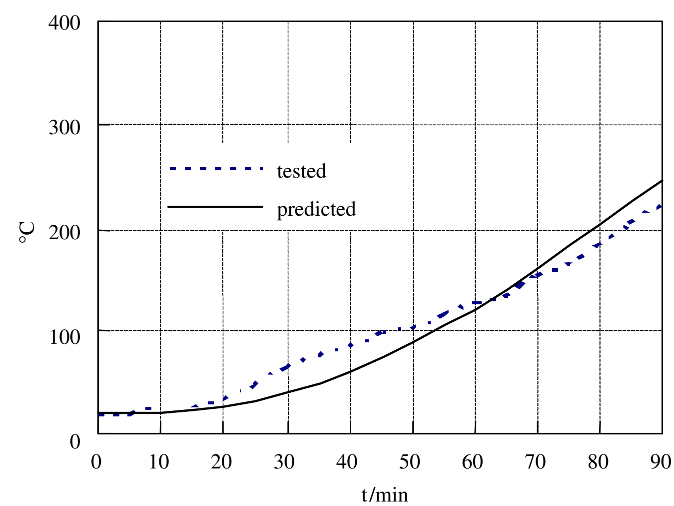

Fig. 10. Comparison of temp–curve (point 5).

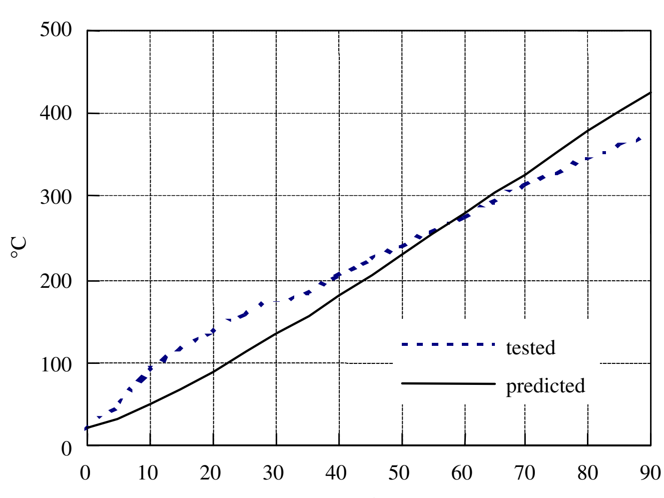

Fig. 8. Comparison of temp–curve (point 3).

3.1. *The coefficients for the heat transfer*

Based on the assumption that the temperatures of a column are uniform along the longitudinal axis, the temperature distribution in the cross-section of a SRC column are regarded as a 2D transient problem. The thermal properties of steel and concrete, such as specific heat and thermal conductivity, which vary with temperature, are defined as follows:

$$C_c = 900 + 80(T/120) - 4(T/120)^2, \quad 20\,^{\circ}\mathrm{C} \leqslant T < 1200\,^{\circ}\mathrm{C}, \tag{3}$$

$$C_s = 425 + 7.73 \times 10^{-1}T - 1.69 \times 10^{-3}T^2 + 2.22 \times 10^{-6}T^3, \quad 20\,^{\circ}\mathrm{C} \leqslant T < 600\,^{\circ}\mathrm{C}, \tag{4}$$

$$C_s = 666 + 13002/(738 - T), \quad 600\,^{\circ}\mathrm{C} \leqslant T < 735\,^{\circ}\mathrm{C}, \tag{5}$$

$$C_s = 545 + 17820/(T - 731), \quad 735\,^{\circ}\mathrm{C} \leqslant T < 900\,^{\circ}\mathrm{C}, \tag{6}$$

$$C_s = 650, \quad 900\,^{\circ}\mathrm{C} \leqslant T < 1200\,^{\circ}\mathrm{C}, \tag{7}$$

in which T is the temperature of a specimen; C_c is the specific heat of concrete and C_s is the specific heat of steel, both expressed in J/kg °C [5,6].

The values of thermal conductivity are defined as follows:

$$\beta_c(T) = 1.6 - 0.16(T/120) + 0.008(T/120)^2, \tag{8}$$

$$\begin{cases} \beta_s = 54 - 3.33 \times 10^{-2}T, & 20\,^{\circ}\mathrm{C} \leqslant T < 800\,^{\circ}\mathrm{C} \\ \beta_s = 27.3, & T \geqslant 800\,^{\circ}\mathrm{C} \end{cases}, \tag{9}$$

in which β_c is the thermal conductivity of concrete and β_s is the thermal conductivity of steel, both expressed in W/(mK) [5,6].

For simplification, several assumptions were made in this study:

1. Since densities of concrete and steel are believed to have little influence on temperature distribution, they are viewed as constants, even though they vary with temperature in many cases.
2. The effect of spalling of concrete is ignored.
3. There is no inner heat source involved for the SRC column.

3.2. Boundary conditions of the SRC columns subjected to fire

Generally a SRC column has two kinds of heat transfer boundary condition when subjected to fire. The first one is the heat flux at the bounding surface, which can be regarded as a simple superposition of convection heat transfer and radiation heat transfer [7].

$$q = q_c + q_r = \alpha_c(T_g - T_s) + \phi\xi\mu_r \times [(T_g + 273)^4 - (T_s + 273)^4]_c, \tag{10}$$

in which q_c and q_r are the convection and radiation heat fluxes at the surface of the SRC column, both expressed in W/m^2; α_c is a convection heat transfer coefficient (W/m^{2}K); T_g and T_s are the temperatures of the furnace and the surface of column respectively; the configuration factor $\phi = 1.0$ and σ is the Stefan–Boltzman constant, the value of which is 5.67×10^{-8}W/(m^{2}K^4); ε_r is the surface emissivity of the column. To the surfaces of the column, which are exposed to a naked flame, the value of ε_r is 0.5, and the value of the other two sides is 0.35.

The second boundary condition is the heat transfer between two kinds of solid materials: concrete and the inner steel section. Besides thermal convection, there are contacting thermal resistances between the interfaces. According to the test data, the temperatures of the inner steel section were seldom higher than 400 °C. In other words, the influence of contacting thermal resistance turns out to be less. As a result, it makes some sense to ignore such effect in the numerical analysis. In addition, we have no reliable materials in this field at present.

3.3. Finite element analysis of the cross-section temperature

The differential equation of thermal convection can be listed as follows [8]:

$$\frac{\partial T}{\partial t} = \frac{\lambda}{\rho C}\left(\frac{\partial^2 T}{\partial x^2} + \frac{\partial^2 T}{\partial y^2}\right), \tag{11}$$

in which x and y are the coordinates, expressed in mm; C is the specific heat; ρ is the density of material.

As to Eq. (11), there is no explicit solution. In this paper, it was solved by a combined method of finite-difference and finite element. The slice of the cross-section (including the steel section) was discretized by triangular elements (Fig. 4). A two-level time discretization method—Galerkin mode was used to approximate the partial derivative $\partial T/\partial t$. In every time step, the former results of temperature distribution act as initial conditions, and the thermal properties of material can be regarded as constants in one element corresponding to the known temperature at the current time iteration. The equation used to calculate T can be listed as follows:

$$T = a_1 + a_2x + a_3y, \tag{12}$$

in which x and y are the coordinates; in one time step, T is a function of x and y, a_1, a_2, a_3 are undetermined coefficients.

The basic equation of transient temperature distribution can be listed as follows [15]:

$$\left(2[K] + \frac{3}{\Delta t}[N]\right)\{T\}_t = (2\{P\}_t - \{P\}_{t-\Delta t}) + \left(\frac{3}{\Delta t}[N] - [K]\right)\{T\}_{t-\Delta t}, \tag{13}$$

in which $[K]$ is a temperature stiffness matrix; $[N]$ is a unsteady temperature-change matrix; $\{P\}$ is a known column vector after the variation of the differential equation.

In Fig. 5 a comparison is shown between the actual temperature curve of the inner furnace and the regression one (Eq. (2)). It also shows five predicted curves corresponding to the locations of five thermocouples. Figs. 6–10 show the details of comparisons between the thermocouples data and those obtained by numerical calculation. Thermocouples 1 and 2 were fixed near the surface of column, therefore they were subjected to much steeper temperature gradient than the others, and the impact of hot air made an additional effect when cracks appeared at the surface of the column. The predictions have generally good agreements with the test data, while small deviations were observed in Figs. 5–10.

4. Nonlinear analysis of the SRC column's ultimate strength

The objectives of the nonlinear analysis are as follows:

1) to obtain the ultimate strength of a SRC column at ambient temperature numerically.
2) to find out the relation between the ultimate strength reduction and various factors at elevated temperatures.

4.1. Assumptions for nonlinear analysis

To carry out the investigation, five assumptions were adopted in developing the procedure:

1) After the formation of cracks, the elevated temperatures have no additional influence on the stress distribution of the SRC column. Actually, by the time the cracks appear, hot air will inevitably have an impact on the inner parts of the column through cracks and cause variation of stress to some degree. It is difficult to predict precisely the appearance of cracks by the numerical method. Therefore the authors have to neglect the influence of temperature distribution on stress in the analysis.
2) there is no load-bond slip between the steel (including steel section and reinforcement) and concrete.
3) plane sections before bending remain plane after bending.
4) simplified assumption of creep and stress [14]. At elevated temperatures creep and stress are coupled, which makes the simulation difficult. When simulating the regime of heating under constant load, it was assumed creep could be deduced directly through the values of stress, which was the result from the previous time step, if the time-steps were small enough. Also in simulating the process of loading under constant temperature, it was assumed creep could be deduced directly by the values of stress, which were also the results of the former load, if the increment of load was small enough.
5) The curvature formula-Eq. (14), given by Lie [9,10], was adopted to simulate the deflection of a SRC column under loads at elevated temperatures. The deflection of an eccentric column interacts with the secondary moment. It will be rather complicated to consider the secondary moment with actual deflection curve. To simplify the problem, the deflection curve of a column was assumed and Eq. (14) was adopted in the simulation:

$$f = \frac{(kL)^2}{12}\frac{1}{\theta}, \tag{14}$$

in which f is the value of deflection (mm); L is the clear height of the SRC column (mm); k is a factor concerned with the value of L; $1/\theta$ is the curvature at the mid-height (mm^{-1}).

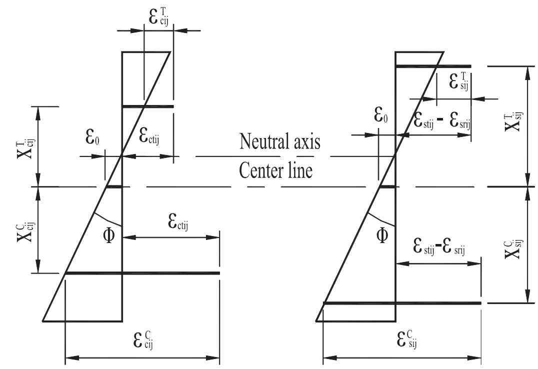

Fig. 11. Strain of concrete.

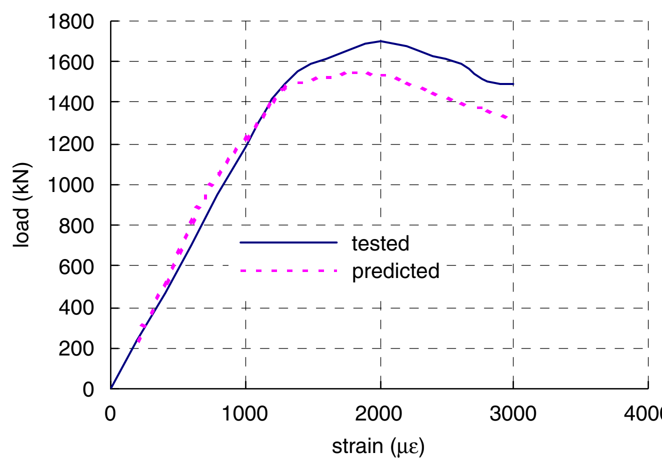

Fig. 12. Comparison of predicted and measured strain of SRC1.4-0 (concrete).

Based on the temperature distribution and stress-strain relation by Lie [9], the strain equations of the cross-section can be deduced as follows (Figs. 11–12):

$$\varepsilon^C_{cij} = \varepsilon_0 + \varphi x^C_{cij} + \varepsilon_{cij}, \tag{15}$$

$$\varepsilon^T_{cij} = \varepsilon_0 - \varphi x^T_{cij} + \varepsilon_{cij}, \tag{16}$$

$$\varepsilon^C_{sij} = \varepsilon_0 + \varphi x^C_{sij} + \varepsilon_{stij} - \varepsilon_{srij}, \tag{17}$$

$$\varepsilon^T_{sij} = \varepsilon_0 - \varphi x^T_{sij} + \varepsilon_{stij} - \varepsilon_{srij}, \tag{18}$$

in which ε^C_{cij}, ε^T_{cij}, ε^C_{sij}, ε^T_{sij} are the strains of concrete or steel in the compressive or tensile region; ε_{ctij} is the comprehensive strain of free thermal expansion and creep; ε_{stij}, ε_{srij} are the strains of thermal expansion and thermal creep of steel, respectively. x^C_{cij}, x^T_{cij}, x^C_{sij}, x^T_{sij} are the distance from the gravity centers of element to the center line; ε_0 is the strain of the element in the center of cross-section; φ is the curvature of cross-section.

It is assumed in this paper that the ultimate strength of the whole SRC column, under loads and fire, is determined by the critical section. In other words, the SRC column loses its load bearing capacity when the critical section fails. Thus, the analysis concentrates on calculating the ultimate strength and deformation of the critical section. With the same subdivision in Fig. 4, the strain of the element can be obtained by the method of iteration.

$$N = \sum_{i=1}^{m}\sum_{j=1}^{n}\left(A_{cij}^{C}\sigma_{cij}^{C} + A_{cij}^{T}\sigma_{cij}^{T} + A_{sij}^{C}\sigma_{sij}^{C} + A_{sij}^{T}\sigma_{sij}^{T}\right), \tag{19}$$

$$M = \sum_{i=1}^{m}\sum_{j=1}^{n}\left(A_{cij}^{C}\sigma_{cij}^{C}x_{cij}^{C} + A_{cij}^{T}\sigma_{cij}^{T}x_{cij}^{T} + A_{sij}^{C}\sigma_{sij}^{C}x_{sij}^{C} + A_{sij}^{T}\sigma_{sij}^{T}x_{sij}^{T}\right), \tag{20}$$

in which A_{cij}^{C}, A_{cij}^{T}, A_{sij}^{C}, A_{sij}^{T} are the areas of concrete or steel elements subjected to compression or tension; σ_{cij}^{C}, σ_{cij}^{T}, σ_{sij}^{C}, σ_{sij}^{T} are the stresses of concrete or steel elements subjected to compression or tension.

4.2. Verification of the procedure

4.2.1. Verification at ambient temperature

In the process of numerical calculation, all the conditions, including section dimensions, material properties, locations and shapes of the steel section and reinforcement etc, were kept the same as those of the specimens (Fig. 11).

As shown in Figs. 12–15, all the predicted results subjected to axial or eccentric loads are in good agreement with the test data before the appearance of the first crack. With the increase in strain, the predicted results become generally greater than the experimental data, but are in an acceptable range. It shows that the finite element models and calculating method adopted are rational and the procedure is capable of predicting the response of a SRC column at ambient temperature.

4.2.2. Verification at elevated temperatures

The authors, when verifying the accuracy of the procedure, adopted the actual temperature–time curve (Eq. (2)) in the numerical calculation.

With the increase in temperatures, the collection and measure of experimental data became more difficult. Even with careful thermal insulation, the strain gauges installed on the reinforcement were damaged after 40 min. Under the protection of concrete, most of the strain gauges installed on the surface of the steel section remained functional throughout the process of tests.

In Figs. 16–19, the results are in excellent agreement with the test data in the first 60 min. The magnitude of deviations increases after that but is always in an acceptable range.

4.2.3. The analysis of deviations between predicted results and test data

1) With the increase in duration time and temperature, differences accumulated in the calculations of temperature distributions and caused greater deviations.

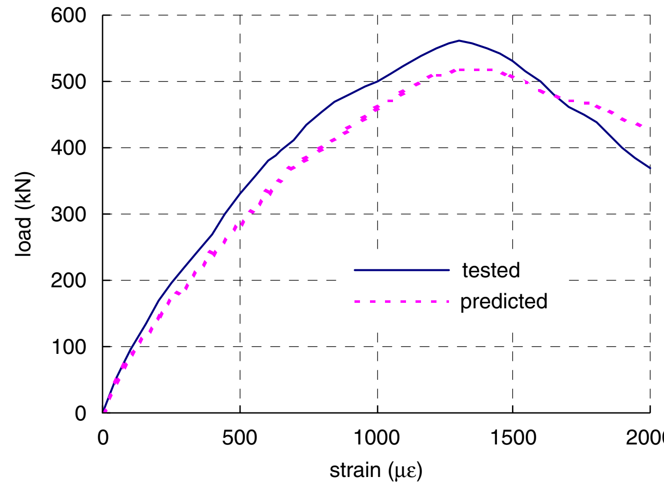

Fig. 13. Comparison of predicted and measured compressive strain of SRC1.8-80 (steel section).

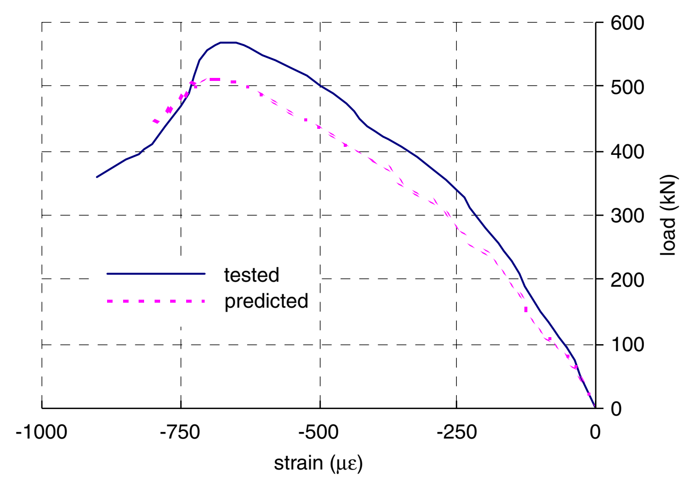

Fig. 14. Comparison of predicted and measured tensile strain of SRC1.8-80 (steel section).

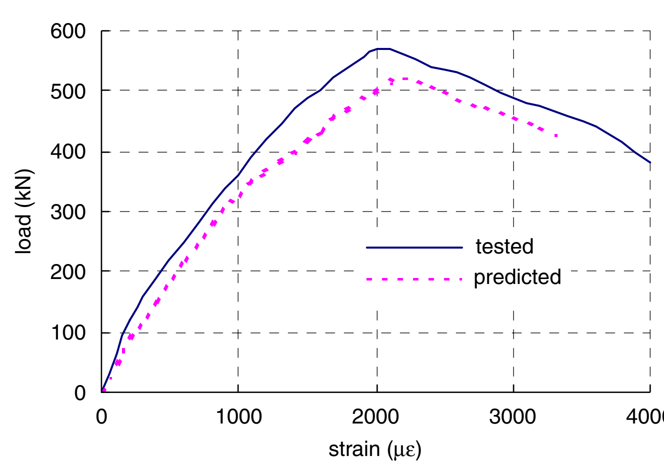

Fig. 15. Comparison of predicted and measured compressive strain of SRC1.8-80 (concrete).

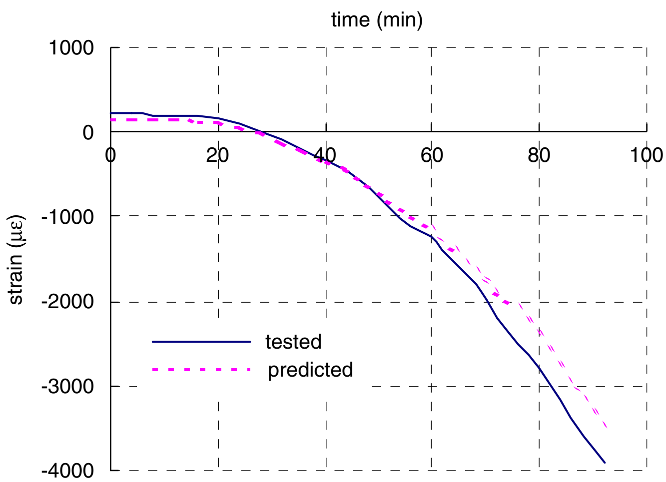

Fig. 16. Comparison of predicted and measured strain versus time of SRC1.4-0 (steel section).

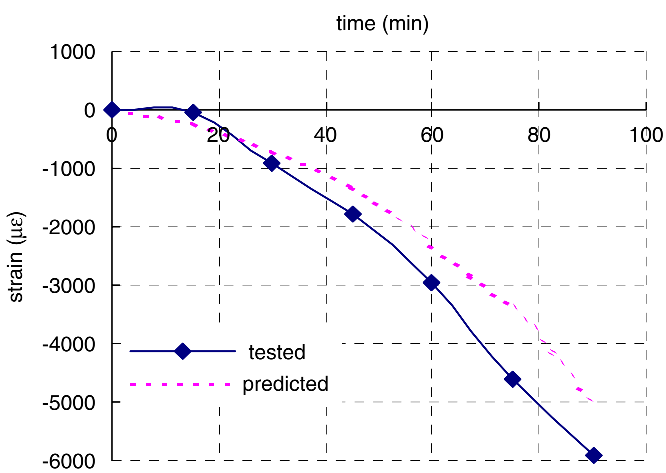

Fig. 17. Comparison of predicted and measured strain versus time of SRC1.8-80 (steel section).

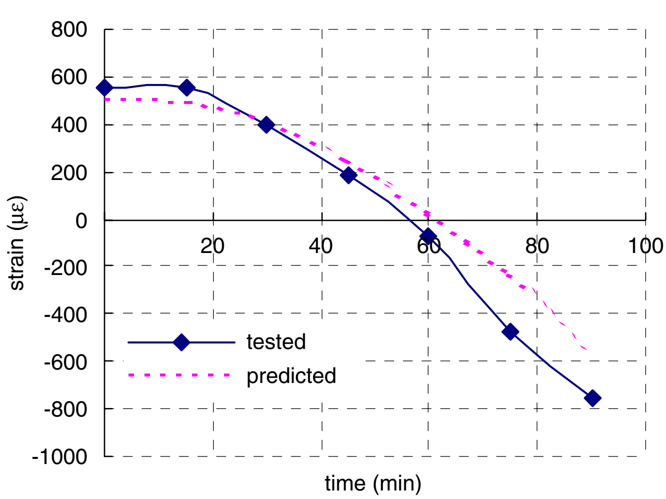

Fig. 18. Comparison of predicted and measured strain versus time of SRC1.8-80 (steel section).

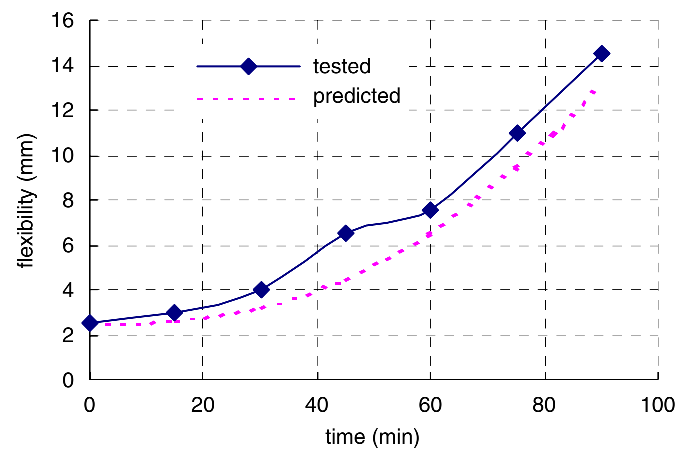

Fig. 19. Comparison of predicted and measured maximum deflection versus time of SRC1.8-80.

2) The complicated ingredients of concrete make it nearly impossible to simulate the actual conditions without any deviation. What is more, this difficulty increases at elevated temperatures;
3) Any slipping, which occurred at the interface of concrete and steel section was neglected. From the investigation of slipping between reinforcement and concrete [11], we knew that the value of increased slipping increased with the temperature. Thus, it is certain that higher temperature will cause greater slipping between the steel section and concrete, which will further increase the deviations.
4) Earlier on the formation of the cracks, hot air brought a sudden temperature rise in the inner part of the SRC column. When the cracks reached the surface of the steel section, significant temperature gradients were observed due to the high thermal conductivity of steel. At present giving a precise prediction of the cracks (appearance time and place, etc.) is still an unachievable goal in our investigation.

In the author's opinion, the second and fourth points are the main causes of the deviations.

4.3. Regression equations of the ultimate strength subjected to the standard fire

Two kinds of loading regimes can be considered by the procedure. Heating under constant load represents the real condition better, while the loading under a constant temperature is proved in investigations [11–13] to lead to a lower value of ultimate strength than the former one. To get comparatively safer equations, the latter loading regime was adopted in deriving the equations of the ultimate strength.

The ultimate strength of a given SRC columns, at ambient temperature, is concerned with diverse factors, such as the initial eccentricity and the adverse effects of long-period loads etc. In the Chinese Code [17], an enhancement coefficient of eccentricity, which was derived by mass experimental data, is adopted to summarize the influence of these factors. Although it is difficult, in a finite element procedure, to simulate all these factors by numerical method, the predictions of the ultimate strength, of which the slenderness ratios are less than 15, were tested to be acceptable. Thus, the equations at elevated temperatures were established by regressing the reduction of the ultimate strength at ambient temperature.

To obtain the reduction caused by elevated temperatures, the data calculated by the procedure were used to derive the ultimate strength equations of the SRC columns by regression.

4.3.1. Equations for the SRC columns subjected to axial load and standard fire

The equation of the ultimate strength under axial load is expressed as follows:

$$N_{ct} = (1 - 4 \times 10^{-6} t^{2.5} + 2 \times 10^{-7} t^3) N_{co}. \tag{21}$$

The equation of corresponding strain of the ultimate strength:

$$\begin{aligned}\varepsilon_{ct} = (1 + 2 \times 10^{-2} t - t^2 + 4.86 \\ \times 10^{-6} t^3 - 2.57 \times 10^{-8} t^4) \varepsilon_{co},\end{aligned} \tag{22}$$

in which t is the duration time; N_{ct} is the ultimate strength of the SRC column subjected to the ISO-834 standard fire at time t, expressed in kN; N_{co} is the ultimate strength of a SRC column at ambient temperature, expressed in kN; ε_{ct} and ε_{co} are the strains corresponding to N_{ct} and N_{co};

4.3.2. Equations for the SRC columns subjected to eccentric load and standard fire

Considering the effect of different slenderness ratios, we write the regression equation in two parts to take this into account:

When $5 \leqslant \lambda < 10$

$$N_{ct} = (1 - 4 \times 10^{-3} t - 2.8 \times 10^{-5} t^2 + 8 \times 10^{-8} t^3) N_{co}, \tag{23}$$

while if $10 \leqslant \lambda < 15$

$$\begin{aligned}N_{ct} = (1 - 2.6 \times 10^{-3} t - 3.26 \times 10^{-5} t^2 + 1.37 \\ \times 10^{-7} t^3) N_{co},\end{aligned} \tag{24}$$

in which t is the duration time; N_{ct} is the ultimate strength with the same slenderness ratio and eccentricity as N_{co} in the ISO-834 standard fire at time t; N_{co} is the ultimate strength of a SRC column at ambient temperature;

4.3.3. The influence of slenderness ratio and eccentricity on the SRC columns in standard fire

There are various factors affecting the ultimate strength of a SRC column subjected to fire. Through analysis, slenderness ratio and eccentricity have been shown to have significant effects.

1) The regression relation between slenderness ratio and ultimate strength

Because of thermal expansion and the variations of material properties, the deformation of a SRC column, under the same load, is significantly greater than that at ambient temperature, especially with a large slenderness ratio.

Knowing that the effect of slenderness ratio has a very different effect during the first 90 min, we write the regression equation in two parts:

When $t \leqslant 90$ min

$$N_{ct} = (0.00113\lambda^3 - 0.033\lambda^2 + 0.29\lambda + 0.2) N_{c7}, \tag{25}$$

while for $90 < t \leqslant 180$ min

$$N_{ct} = (1 - 0.0002\lambda^3 + 0.0042\lambda^2 - 0.084\lambda + 1.45) N_{c7}, \tag{26}$$

in which N_{ct} is the ultimate strength of a SRC column at the same duration time as N_{c7}; λ is a slenderness ratio no more than 15; N_{c7} is the ultimate strength of a SRC column with $\lambda = 7$ at given time.

2) The regression relation between eccentric ratio and ultimate strength.

Because the numerical analysis could not simulate the inevitable geometrical imperfections directly, an additional initial eccentricity of 20 mm, according to the Chinese Code [16], was adopted to substitute for the imperfections.

While $t \leqslant 90$ min

$$N_{ct} = (-5.25\eta_e^3 + 7.46\eta_e^2 - 4.33\eta_e + 1.36) N_{20}. \tag{27}$$

For $90 < t \leqslant 180$ min

$$N_{ct} = (-6.31\eta_e^3 + 8.22\eta_e^2 - 4.29\eta_e + 1.35) N_{20}, \tag{28}$$

in which N_{ct} is the ultimate strength of a SRC column at the same time as N_{20}; η_e is the eccentric ratio, $\eta_e = e_0/H$; N_{20} is the ultimate strength of a SRC column with the eccentricity set to 20 mm at the given time.

5. Conclusions

The PTDD procedure was developed to predict the temperature distribution and responses of a SRC column subjected to fire and loads. In this procedure, a structural member was divided into elements, and time was discretized into steps. The temperature distribution was calculated by a combined method of finite-difference and finite element. The predictions of ultimate strength at elevated temperatures were obtained by an iterative calculation. The complex features of structural behavior at elevated temperatures, such as thermal expansion, creep and material properties changing with temperatures were considered in the model. Conclusions derived from the study include the following:

1) by comparing the predictions and the test data, the predicted results of temperature distribution calculated by the finite element method was found to be satisfactory.
2) compared with the test data, the calculated results of the response of the columns subjected to fire, such as the strain and deflection, obtained by the procedure showed satisfactory agreement both at ambient temperature and elevated temperatures.
3) there is no simple relationship for the fire-resistance analysis of the SRC columns. Shape and dimension of cross-section, appearance of cracks, slenderness ratio and eccentricity etc, all couple with the temperature regime and affect the fire resistance of the SRC column. The equations obtained by regression analysis are valid only for the conditions described in the paper. Further investigations are necessary to extend the work to more general conditions.

Acknowledgements

The research work reported here was made possible by the state laboratory of disaster reduction in Tongji University. The financial support is highly appreciated. The authors also express special thanks to Dr. Zhao-Hui Xu, Dr. Shou-Chao Jiang and Dr. Dong-hong Jiang for their assistance.

References

[1] GB2975 Test standard for steel material. Peking: Chinese Planning Press; 1982.
[2] GBJ81-85 Test standard for concrete material. Peking: Chinese Planning Press; 1985.
[3] ISO-834 Fire resistance test-elements of building construction. International Standard ISO384, Geneva, 1975.
[4] GB9978-88 Test standard for fire resistance of construction members. Peking: Chinese Planning Press; 1988.
[5] CEN: DAFT ENV 1993. Euro code 2: Design of Concrete Structures.
[6] CEN: DAFT ENV 1993. Euro code 3: Design of Steel Structures
[7] Incropera FP, Dewitt DP. Fundamentals of heat and mass transfer. Wiley; 1985.
[8] Jaluria Y, Torrance KE. Computational heat transfer. Washington, DC: Hemisphere Pub Corp.; 1986.
[9] Lie TT. Fire resistance circular steel columns filled with bar-reinforced concrete. J Struct Eng 1994;120(5):1489–509.
[10] Lie TT, Celikkol B. Method to calculate the fire resistance of Circular reinforced concrete columns. ACI Mater J 1991;88(1):84–91.
[11] Guo Z-H, Shi X-D. The property and calculation method of reinforced concrete at elevated temperatures. Tsinghua University Press; 2003.
[12] Shengrui L, Zhenhai G. Experimental investigation of multiaxial compressive strength of concrete under different stress paths. ACI Mater J 1997;94(5):427–34.
[13] Khoury GA, et al. Transient thermal strain of concrete: literal review, conditions within specimen and behavior of individual constituents. Mag Concrete Res 1985:131–43.
[14] Khoury GA, Majorana CE, Pesavento F, Schrefler BA. Modeling of heated concrete. Mag Concrete Res 2002;54(2):77–101.
[15] Xiang-qian K. The application of the finite element method in heat transfer. China: The Press of Science; 1998.
[16] GB 50010-2002. Code for design of concrete structure. PR China: Ministry of Construction; 2004.
[17] JGJ 138-2001. Technical specification for steel reinforced concrete composite structures. PR China: Ministry of Construction; 2002.